How to cite: *Angew. Chem. Int. Ed.* **2021**, *60*, 4789–4795
International Edition: doi.org/10.1002/anie.202013811
German Edition: doi.org/10.1002/ange.202013811

Metal-Organic Frameworks

Persistent Radical Tetrathiafulvalene-Based 2D Metal-Organic Frameworks and Their Application in Efficient Photothermal Conversion

Jian Su[+], Ning Xu[+], Ryuichi Murase, Zhi-Mei Yang, Deanna M. D'Alessandro, Jing-Lin Zuo, and Jia Zhu**

Dedicated to the 100th anniversary of the School of Chemistry and Chemical Engineering, Nanjing University

Abstract: *A series of stable radical 2D metal-organic frameworks has been assembled. $(m\text{-TTFTB})_3$ (m-Tetrathiafulvalene-tetrabenzoate) trimer building blocks are beneficial for the stability of the radicals due to delocalization of the unpaired electron. Hexanuclear rare-earth-cluster-based 1D chains further enhance the stability of the frameworks. The radical state of the middle TTF in the trimer has been observed by the change of central C–C and C–S bond distances and the configuration of the TTF by single-crystal X-ray diffraction. The radical characteristics are also confirmed by electron paramagnetic resonance, UV/Vis–NIR absorption, and X-ray photoelectron spectroscopy experiments. Stability tests showed that the radicals are stable even in solutions and under acid/base environments (pH 1–12). Owing to efficient light absorption due to intramolecular charge transfer, low thermal conductivity, and outstanding stability, the radical 2D Dy-MOF shows excellent photothermal properties, an increase of 34.7°C within 240 s under one-sun illumination.*

Introduction

Organic radicals, these being species with unpaired electron(s), are essential to a plethora of chemical and biological activities on account of their distinctive chemical bonding and physical properties (magnetic, electrical, optical, etc.), as well as their emerging applications as functional materials.[1] The oxygen molecule (O_2) for example, is one of the simplest radical species which exists in the atmospheric environment. With regard to synthesized radical organic molecules, nitroxide, triphenylmethyl, phenalenyl, verdazyl, and dithiadiazolyl are seen as common families of persistent organic radicals. However, most of the main group radicals are frequently transient as the unpaired electrons make them highly reactive.[1a] Two strategies have been introduced to stabilize the main group radicals. One involves the use of bulky groups to prevent oligomerization (kinetic stabilization). A second involves delocalization of the unpaired electron (thermodynamic stabilization). These strategies are very beneficial for the generation, observation, and in some cases, isolation of radicals.[1a] The successful synthesis of persistent organic radicals has enabled the application of organic radicals as building blocks for functional molecular materials.[2] In the development of multi-functional materials, inorganic-organic hybrid materials could provide a powerful platform to incorporate both a designable persistent organic component and a functional inorganic component.

Metal-organic frameworks (MOFs) exhibit many advantages including reticular synthesis, ordered crystallinity and porosity, as well as myriad functional applications. By exploiting MOFs as a functional platform, radical organic linkers can be well-dispersed in a periodic arrangement.[3] On the one hand, considering the stability of the frameworks, strong coordination bonds with highly linked, cluster-based inorganic secondary building blocks are adopted.[4] With regard to the various types of cluster MOFs, RE_6-MOFs (RE: rare earth) are similar to the now archetypal zirconium-MOFs, and have been investigated for their reticular synthesis, post-synthetic modification and functional applications.[5] In 2013, Eddaoudi et al. first reported a series of MOFs constructed from the 12-connected hexanuclear rare-earth-based secondary building block $[RE_6(\mu_3\text{-}OH)_8(H_2O)_6(O_2C\text{-})_{12}]$.[6] Furthermore, the applications of these MOFs have been expanded to gas adsorption,[6,7] separation,[8] and catalysis.[9] On the other hand, based on the easy-tailorability and functionality of the organic linkers, organic radical linkers can be stabilized by delocalization of the unpaired electron into a conjugated system. Addressing the challenge of stabilizing radicals within frameworks is an important goal.

Tetrathiafulvalene (TTF) is well known for its two easily accessible and reversible oxidation states (i.e. $TTF^{\bullet+}$ radical cation and TTF^{2+} dication) that has been extensively studied as an important electron donor component for conductive,[10] optoelectronic,[11] magnetic,[12] catalysis,[13] and intelligent

[*] Dr. J. Su,[+] Z. Yang, Prof. Dr. J. Zuo
State Key Laboratory of Coordination Chemistry, School of Chemistry and Chemical Engineering, Collaborative Innovation Center of Advanced Microstructures, Nanjing University
Nanjing 210023 (P. R. China)
E-mail: zuojl@nju.edu.cn
Dr. N. Xu,[+] Prof. Dr. J. Zhu
National Laboratory of Solid State Microstructures, Collaborative Innovation Center of Advanced Microstructures, College of Engineering and Applied Sciences, Nanjing University
Nanjing 210023 (P. R. China)
E-mail: jiazhu@nju.edu.cn
Dr. R. Murase, Prof. Dr. D. M. D'Alessandro
School of Chemistry, The University of Sydney
Sydney, New South Wales, 2006 (Australia)
[+] These authors contributed equally to this work.
Supporting information and the ORCID identification number(s) for the author(s) of this article can be found under: https://doi.org/10.1002/anie.202013811.

porous materials.[14] In the oxidation of TTF to $TTF^{\bullet+}$, one of the 7π-electron dithiolylidene rings in the TTF converts to an aromatic 6π-electron configuration. This rigid and fully conjugated aromatic 6π-electron ring is capable of stabilizing a radical. Moreover, in the reported works, TTF derivatives have already been shown to exist in the $TTF^{\bullet+}$ oxidized state by in situ synthesis,[15] post-synthetic modification,[12a,c,13a,14a] and electrochemical synthesis.[16] Thus, in the present case the TTF moiety was selected as a conjugated aromatic system to stabilize the radical in the framework. Although several radical MOFs have been reported,[3,17] persistent radical MOFs with atomically-resolved structures and stability under harsh conditions have received limited attention. With regards to functional applications, the introduction of radicals into the conjugated molecules will promote a bathochromic shift in the absorption and hence enhance the photothermal efficiency. The use of clean solar energy and its efficient conversion have enormous economic, environmental and societal benefits. Thus, the combination of MOF structural diversity and the beneficial characteristics of radicals have enormous prospects.

Herein, we report the synthesis of a series of two-dimensional radical MOFs generated from the $(m\text{-TTFTB})_3$ (*m*-tetrathiafulvalene-tetrabenzoate, Scheme S1) trimer secondary building units (SBU) and hexanuclear RE clusters by the use of solvothermal in situ synthesis. The framework consists of 14-connected RE_6 clusters where the formate ions are linked to form an infinite one-dimensional chain. Notably, the in situ generated $TTF^{\bullet+}$ was confirmed by X-ray diffraction and a characteristic EPR signal. Furthermore, the two-dimensional MOFs denoted **RE-2D**, $[RE_6(m\text{-TTFTB})_{2.5}(\mu_3\text{-OH})_8(H_2O)_2(HCOO)_2]\cdot 1.5\,(NH_2(CH_3)_2)\cdot 5\,DMF\cdot 8\,H_2O$ where RE = **Tb**, **Dy**, and **Er**), are found to perform as photothermal conversion materials with the existence of charge transfer, low thermal conductivity, and favourable solar absorption.

Results and Discussion

Crystal Structures of 2D Radical MOFs

Frameworks assembled from H_4TTFTB and diverse metal ions have been reported over the years with various applications.[11a,12,13,14b,15b,18] The Zn_2(TTFTB) framework has shown a rare stacked structure and high intrinsic charge mobility.[18a] With consideration for the low-dimensional structure and molecular assembly of the TTF SBU, a new ligand, *m*-H_4TTFTB, similar to H_4TTFTB was recently synthesized.[10a] Herein, a series of two-dimensional radical MOFs, named **Tb-2D**, **Dy-2D**, and **Er-2D** ($[RE_6(m\text{-TTFTB})_{2.5}(\mu_3\text{-OH})_8(H_2O)_2(HCOO)_2]\cdot 1.5\,(NH_2\text{-}(CH_3)_2)\cdot 5\,DMF\cdot 8\,H_2O$), have been successfully assembled from the rare earth metal ions and the *m*-H_4TTFTB ligand. Although **Er-2D** was obtained only as microcrystalline powders, the X-ray diffraction patterns of the single crystal and powder revealed that these isostructural two-dimensional MOFs are crystallized in the triclinic space group $P\bar{1}$ (Table S1). The asymmetric unit (Figure S1) of **Dy-2D** contains three Dy^{3+} ions, one and a quarter of *m*-$TTFTB^{4-}$, one coordinated H_2O, four coordinated μ_3-OH, and one coordinated formate ion ($HCOO^-$). The *m*-$TTFTB^{4-}$ ligand coordinates to eight Dy^{3+} ions with its eight oxygen atoms in a mono-dentate mode (Figures S2a,b). There are three kinds of crystallographically unique Dy^{3+} ions in the Dy_6 cluster of the crystal structure (Figures S2c,d,e). The Dy1 and Dy2 ions located at the horizontal plane of the Dy_6 cluster are both eight coordinate involving four μ_3-OH, one formate, and three carboxylate groups from three *m*-$TTFTB^{4-}$ where all are in a mono-dentate mode. The vertical Dy3 ion is nine coordinate involving four μ_3-OH, one water, and four carboxylate groups from four *m*-$TTFTB^{4-}$ ligands where all are in mono-dentate modes. In total, the connectivity number of the Dy_6 cluster is 14, in which ten are from *m*-$TTFTB^{4-}$ carboxylate groups and four are from coordinated formates (Figure S3a). In the $Dy_6(\mu_3\text{-OH})_8$ core, μ_3-OH groups are coordinated on the eight triangle faces of the slightly distorted octahedron (Figure 1e). The distance between adjacent Dy···Dy ions is in the range 3.853–3.994 Å (Figure S3b). The Dy−O bond lengths are in the range 2.278 to 2.582 Å, which are consistent with those reported for Dy compounds.[12b,c] The adjacent Dy_6 clusters are bonded by two formates to generate a one-dimensional (1D) chain-like structure (Figure 1d). The 1D chain is connected by the eight-coordinated *m*-$TTFTB^{4-}$ ligand forming a 2D framework (Figure 1g). These 2D layers were connected by weak interactions to form a 3D structure (Figure S4). The SQUEEZE calculations from PLATON[19] give a total solvent-accessible volume of 740.1 $Å^3$ per unit cell, corresponding to 25.7% of the total crystal volume of **Dy-2D**. The volume for **Tb-2D** differs slightly, with 745.5 $Å^3$ (25.7%) per unit cell. The ideal N_2 sorption was not obtained owing to various weak interactions between the frameworks and DMF molecules and the small window of the caves that prevent the export of DMF molecules (Figure S5).

Notably, in the single crystal structure, there is a sandwich-type TTF trimer within which the distance between adjacent TTFs is 3.703 Å (Figure 1a). To understand the oxidation state of each TTF in the trimer of **Dy-2D**, their geometry and bond parameters were analyzed in detail (Figure 1c and Tables S2 and S3).[16] The two external TTFs are in boat style conformations and the central TTF is planar, indicating different oxidation states. In the two external TTFs, the central C−C and average C−S bond distances are 1.352 Å and 1.764 Å, respectively. These bond parameters are consistent with the reported values of neutral TTF.[12c,14b,18b] In contrast, in the central TTF, the central C−C and averaged C-S bond distances are 1.392 Å and 1.749 Å, respectively. The elongated C−C distances and shortened C-S distances indicate that the central TTF is in the radical cation state, $TTF^{\bullet+}$.[16]

Radical and Electrical Conducting Properties

The phase purity of **Tb-2D**, **Dy-2D**, and **Er-2D** was confirmed by powder X-ray diffraction (PXRD) measurements in which the positions of diffraction peaks were consistent with those calculated from single-crystal X-ray diffraction data (Figures 2a and S6). Thermogravimetric

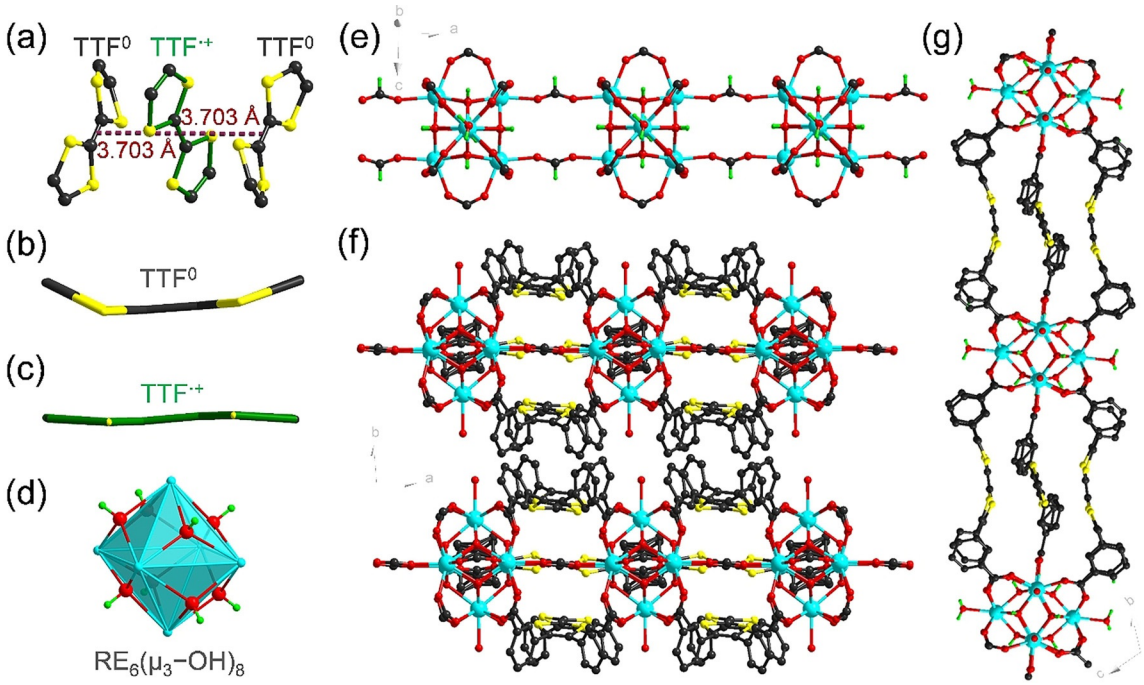

Figure 1. Structural analysis of **Dy-2D**. a) The distance between TTF moieties in the trimer. b) The geometry of the peripheral TTF in the trimer. c) The geometry of the middle TTF in the trimer. d) Dy_6 cluster capped by eight face μ_3-OH. e) One-dimensional chain constructed from Dy_6 clusters and $HCOO^-$. f) View of the three-dimensional framework along the ***c*** direction. g) The two-dimensional framework viewed along the ***a*** direction. Color Scheme: Dy, cyan; O, red; C, black; S, yellow; H, green.

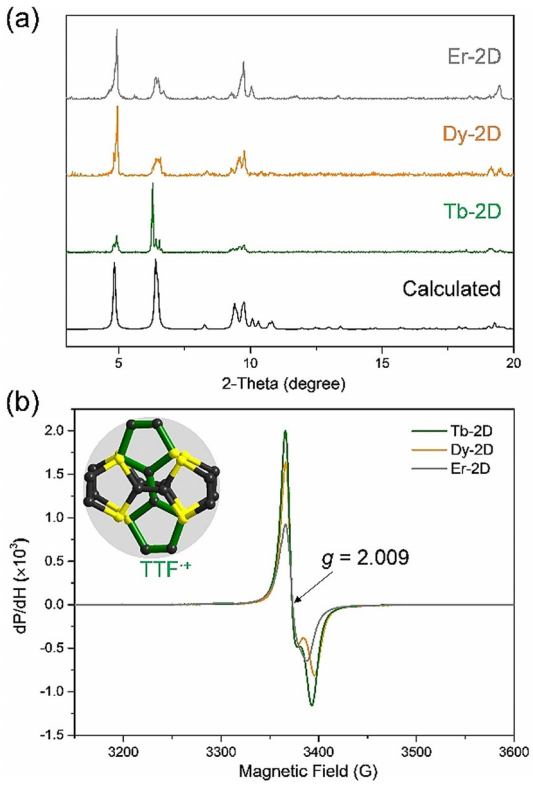

Figure 2. Characterization of 2D radical MOFs. a) Calculated and experimental powder X-ray diffraction results for **Tb-2D**, **Dy-2D**, and **Er-2D**; b) the EPR spectra of solid-state samples of **Tb-2D**, **Dy-2D**, and **Er-2D** at 110 K.

analysis (TGA) of **Tb-2D**, **Dy-2D**, and **Er-2D** shows that these frameworks can be desolvated at 360 °C (Figure S7). The continuous-wave electron paramagnetic resonance (CW-EPR) spectra of the frameworks exhibit a strong resonance at $g = 2.009$, which is assigned to $TTF^{\bullet+}$ in the trimer (Figure 2b).[12a,14a] To assess the electronic effects of the $TTF^{\bullet+}$ radical and the trimer building block in these frameworks, electrical conductivity characterization was measured with pelletized samples at room temperature. The electrical conductivities are 1.8×10^{-8}, 3.0×10^{-8}, and 7.1×10^{-8} S cm^{-1} for **Tb-2D**, **Dy-2D**, and **Er-2D**, respectively (Figures S8–S10 and Table S4). Despite the existence of the $TTF^{\bullet+}$ cation radical in the framework, the lack of orbital overlap among the trimers prevents inter-trimer charge transport, resulting in low electrical conductivities.[12a,c,14a]

Cyclic Voltammetry and Diffuse Reflectance Spectra

To understand the redox properties of these three frameworks, their solid state cyclic voltammograms (CVs) and differential pulse voltammograms (DPVs) were measured in 0.1 M $TBAPF_6$/MeCN. The representative voltammogram of **Dy-2D** taken at 100 mV s^{-1} is shown in Figure 3a. Upon cycling anodically, two broad processes appear at 0.11 and 0.47 V (vs. Fc/Fc^+), which are attributed to the $TTF/TTF^{\bullet+}$ and $TTF^{\bullet+}/TTF^{2+}$ redox couples, respectively. These processes are more clearly observed in the DPV of **Dy-2D**. At higher scan rates (> 400 mV s^{-1}), the Faradaic processes become indistinguishable due to the large capacitive current (Figure 3b). CVs of **Tb-2D** and **Er-2D**, are shown in Figures S9a and S10a, respectively. In both of these cases, the two one-

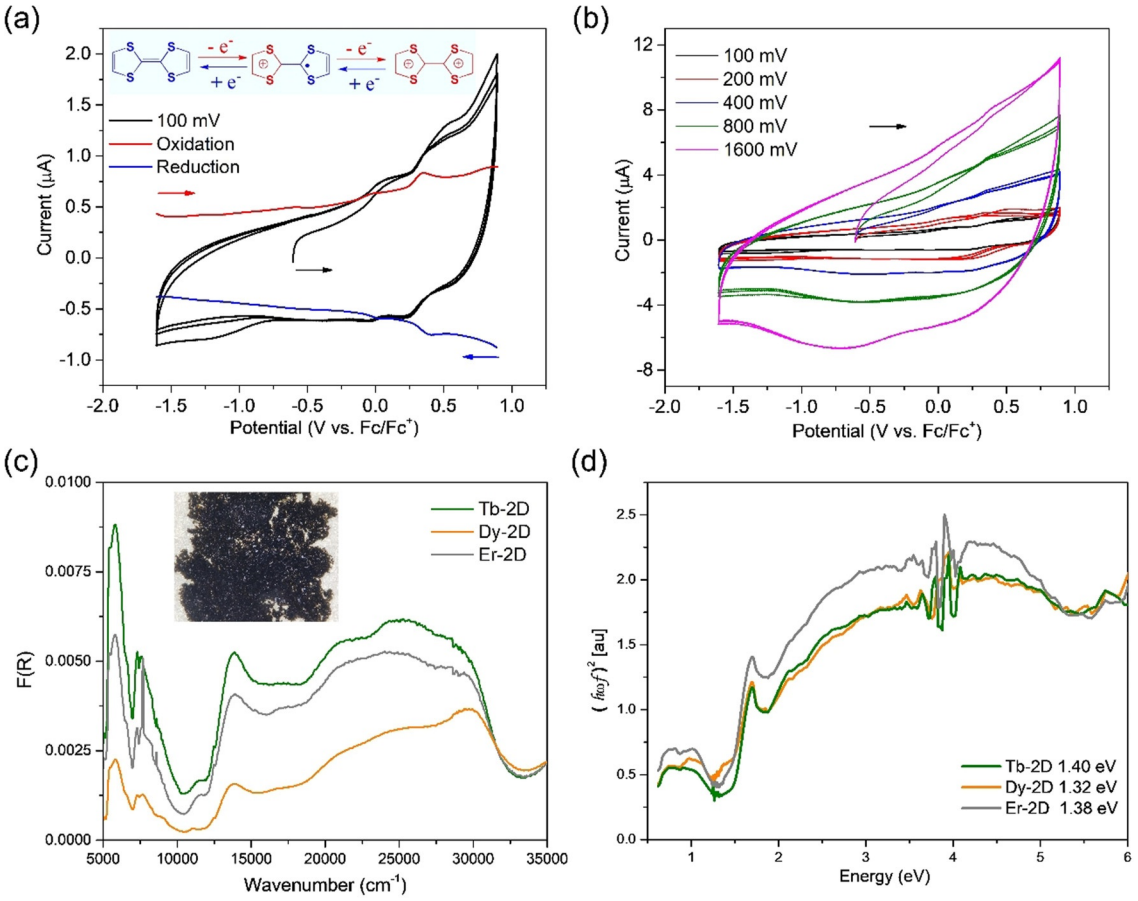

Figure 3. Solid state cyclic voltammetry and diffuse reflectance spectra of 2D radical MOFs. a) Cyclic (black line) and differential pulse voltammograms (red and blue lines) of **Dy-2D** at 100 mV s^{-1}. The inset shows the oxidation and reduction processes described in the CV. b) The CVs of **Dy-2D** over three consecutive cycles at different scan rates. The experiments were conducted in 0.1 M $TBAPF_6$/MeCN electrolyte. c) Normalized diffuse reflectance spectra of **Tb-2D**, **Dy-2D** and **Er-2D**. The inset is a photograph of **Dy-2D** crystals. d) Tauc plots of **Tb-2D**, **Dy-2D** and **Er-2D**.

electron oxidation reactions attributed to the TTF/TTF$^{\bullet+}$ and TTF$^{\bullet+}$/TTF^{2+} redox couples were also observed (0.11 and 0.47 V (vs. Fc/Fc$^+$) for **Tb-2D**; 0.13 and 0.67 V (vs. Fc/Fc$^+$) for **Er-2D**). Additionally, faster sweep rates resulted in broad features as a result of slow diffusion kinetics through the framework structure (Figures S11b and S12b). Finally, in all compounds, a voltammogram of the bare electrode following the solid state cyclic voltammetry experiment (i.e., after the solid had been removed from the electrode) revealed very minute signs of dissolution (Figure S13).

The solid state diffuse reflectance spectra for **Tb-2D**, **Dy-2D**, and **Er-2D** are shown in Figure 3c. The spectrum of **Dy-2D** shows five bands at 5760, 7530, 13740, 20890 and 29810 cm^{-1}. The band at 13740 cm^{-1} is attributed to TTF$^{\bullet+}$, further confirming its presence. The bands in the ultraviolet (UV) region are assigned to intramolecular charge transfer (ICT) transitions arising from the *m*-TTFTB ligand. Given the presence of mixed-valence TTF$^{0/\bullet+}$ within a TTF trimer, the two near infrared (NIR) transitions (5760 and 7530 cm^{-1}) are attributed to intervalence charge transfer (IVCT) bands, akin to those found in the related system.[12c] For **Tb-2D** and **Er-2D**, almost identical features were observed. With the UV-vis-NIR adsorption data, we estimated the optical band gaps of **Tb-2D**, **Dy-2D**, and **Er-2D** by the Kubelka-Munk function and Tauc plots, which reveal 1.40, 1.32, and 1.38 eV for **Tb-2D**, **Dy-2D**, and **Er-2D**, respectively (Figure 3d). The optical band gaps of these MOFs are smaller than those reported for RE-TTFTB ($\approx$1.8 eV) and are comparable to those reported for radical TTF-based frameworks ($\approx$1.1 eV).[12c]

Stability of the Radical 2D-MOF

It is known that stability is a limitation in the application of MOFs.[4] PXRD measurements were first conducted to check the stability of the TTF$^{\bullet+}$ in the framework. After being soaked in common organic solvents and water for 24 hours without stirring, **Dy-2D** retains its structure, as indicated by consistent PXRD patterns (Figures S14 and S15). To further study the stability in acidic/basic environments, **Dy-2D** was immersed in aqueous solutions at various pH values for 24 hours without stirring. To examine the stability of **Dy-2D**, the supernate was measured by the inductively coupled plasma atomic emission spectroscopy (ICP-AES, Table S5). The leaching Dy and S atoms are determined to be <0.5 wt % (pH 1) and <0.07 wt % (pH 1, 12), respectively. While the

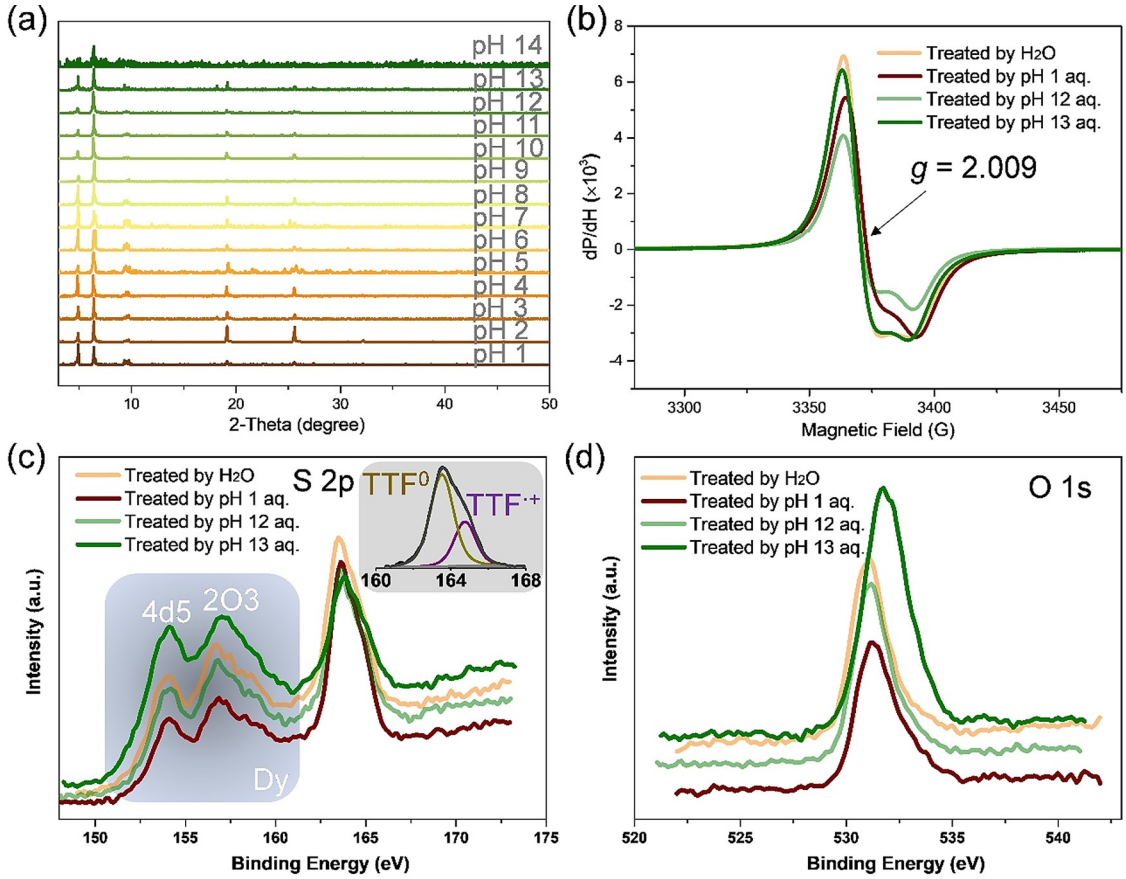

Figure 4. Stability of **Dy-2D** radical MOFs in acidic and basic environments. a) Observed powder X-ray diffraction patterns for **Dy-2D** at different pH conditions (aq.), b) the EPR spectra of solid-state samples of **Dy-2D** treated under different conditions and measured at 110 K. The XPS spectra of S 2p (c) and O 1s (d) of **Dy-2D** treated under different conditions. The inset in Figure 4c is the simulation of S2p divided by TTF^0 and $TTF^{\bullet+}$.

leaching S atoms are determined to be 1.3 wt% (pH 13). These results indicate that this material can be stable in the pH range of 1–12. The PXRD and Fourier transform infrared spectrometry (FT-IR) (Figure S16) results of the solid samples confirm that this material retains its structure in the pH range of 1–12 (Figure 4a). This exceptional stability originates from the infinite one-dimensional chain incorporating the 14-connected RE_6 clusters (Figure 1d) and the tightly bound TTF trimers (Figure 1a). The unaltered state of $TTF^{\bullet+}$ in the TTF trimer was confirmed by the EPR signals of the treated samples (Figure 4b). In order to gain a deep understanding of the atomic information of the samples treated by strong acid/base, X-ray photoelectron spectroscopy (XPS) was conducted (Figure S17). The similar C 1s, S 2p, Dy 4d5 and Dy 2O3 spectra of **Dy-2D** under various conditions confirm the stability of the ligand and the partial radical component (Figure 4c and Figure S18). Furthermore, the S 2p band can be deconvoluted into two bands that are assigned to TTF^0 (163.5 eV) and $TTF^{\bullet+}$ (164.8 eV) (Figure 4c), respectively.[12a,20] It is worth nothing that the O 1s spectrum of the sample treated in pH 13 aqueous solution differs from others (Figure 4d). This change is rationalized by the dissociation of the coordinated carboxylates and the formation of free carboxylates, indicating the partial decomposition of the framework at pH 13. In summary, the TTF radicals and the frameworks show good stability in organic/aqueous solution and rigorous acidic/basic environments (pH 1–12).

Photothermal Conversion of the Radical 2D-MOF

Considering the efficient visible and NIR absorption in addition to the excellent stability of these radical MOFs, **Dy-2D** was expected to possess excellent performance for photothermal conversion. The **Dy-2D** sample was illuminated with simulated sunlight to investigate its photothermal properties with respect to potential practical applications. Under illumination with 1-sun (0.1 W cm^{-2}, 280–2500 nm), the temperature of the radical MOF powders increases rapidly, as monitored by an IR camera. As shown in Figure 5a, once the light was on, the temperature of the radical MOF sharply increased and reached a maximum of 63.9 °C in 240 s (increasing 34.7 °C). The radical MOF sample then entered a quasi-steady-state, which showed an additional temperature increment of 1.7 °C in another 240 s (Figure S19). Because of the existence of $TTF^{\bullet+}$ in the TTF trimer, the significant effect resulting from ICT and IVCT plays a key role to enhance efficient light absorption.[21] In addition, strong TTF interactions in the TTF trimer as well as π-electron delocalization are beneficial for the photothermal

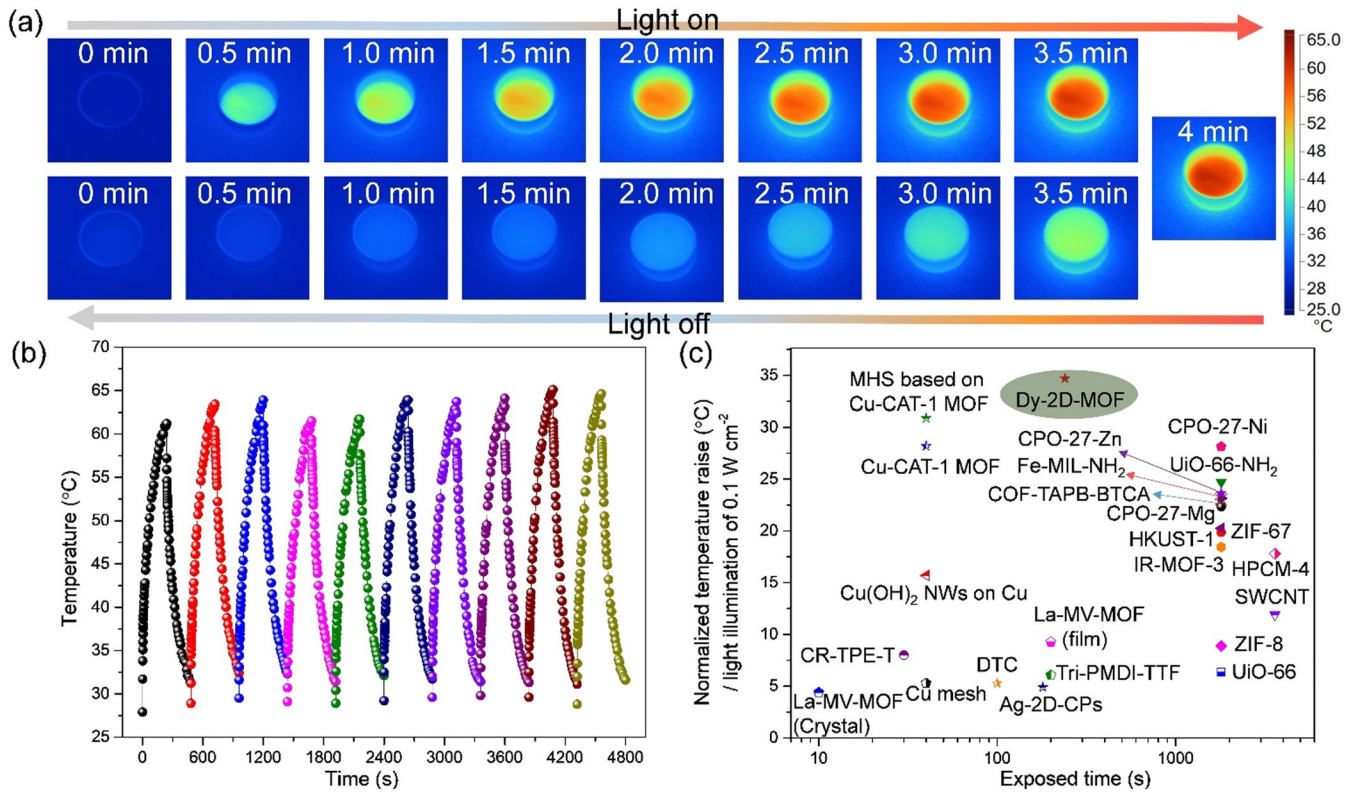

Figure 5. Photothermal conversion of **Dy-2D** radical MOFs. a) The IR thermal images of **Dy-2D** radical MOF powder (≈250 mg) under one unit sunlight irradiation (0.1 Wcm^{-2}) which was then turned off. b) Anti-photobleaching property of **Dy-2D** radical MOF powder during ten heating-cooling cycles. c) The temperature raise for various photothermal materials normalized by light illumination of 0.1 Wcm^{-2}. The photothermal property in this work approximately compared with previous results of solid materials in the literatures.

conversion. These characteristics suppress the photon emission process and improve photothermal efficiency. Additionally, the combination of the organic linkers and the cluster-based inorganic SBU contribute to the relatively low thermal conductivity, which is ideal for photothermal localization.[22] All these features clearly result in the excellent photothermal conversion performance of these radical MOFs. Compared with other solid materials, this 2D radical MOF shows the first-rate photothermal conversion performance under 1-sun (0.1 $W cm^{-2}$) relative to MOFs known at present (Figure 5c and Table S6).[23] Moreover, the cyclic test (Figure 5b) illustrates the good photo-stability of these radical MOFs. After ten repeated illumination cycles, the average temperature rapidly reaches 63.3 °C (with an average increase of 34.2 °C) in 240 seconds. Finally, the PXRD patterns and the XPS results after the cycling experiments also provide evidence of its stability (Figures S20 and S21). These advantages offer possibilities for further photothermal applications, such as photothermal organic catalysis, photothermal therapy, water steam generation, and seawater treatment.

Conclusion

The synthesis of persistent radical MOFs with functional applications remains a highly significant challenge. The combination of radical $(m\text{-TTFTB})_3$ trimer SBU and hexanuclear RE cluster-based infinite one-dimensional chains has resulted in a series of radical MOFs which are stable in nonaqueous/aqueous solutions and in acid/base environments (pH 1–12). Benefiting from intramolecular charge transfer, low thermal conductivity, as well as excellent stability, the radical **Dy-MOF** shows excellent photothermal conversion with an increase of 34.7 °C upon irradiation by one unit of sunlight within 240 seconds. We believe our work will stimulate further studies on persistent radical MOFs for applications in photothermal conversion, and may expand their future applications into the areas of solar energy utilization, photothermal therapy, seawater desalination and so on.

Acknowledgements

This work was supported by the National Basic Research Program of China (2018YFA0306004 and 2017YFA0205700), the National Natural Science Foundation of China (21875099, 21631006 and 51925204), the Australian Research Council (FT170100283), the Fundamental Research Funds for the Central Universities (021314380179). The authors are grateful to Dr. Lei Sun in Argonne National Laboratory for his help on this work.

Conflict of interest

The authors declare no conflict of interest.

Keywords: crystal structures · metal-organic frameworks · photothermal conversion · radicals · redox activity

[1] a) P. P. Power, *Chem. Rev.* **2003**, *103*, 789 – 810; b) Z. Ma, K. T. Mahmudov, V. A. Aliyeva, A. V. Gurbanov, A. J. L. Pombeiro, *Coord. Chem. Rev.* **2020**, *423*, 213482; c) Y. Su, R. Kinjo, *Coord. Chem. Rev.* **2017**, *352*, 346 – 378; d) I. Ratera, J. Veciana, *Chem. Soc. Rev.* **2012**, *41*, 303 – 349; e) M. Abe, *Chem. Rev.* **2013**, *113*, 7011 – 7088; f) M. Mas-Torrent, N. Crivillers, C. Rovira, J. Veciana, *Chem. Rev.* **2012**, *112*, 2506 – 2527.

[2] a) J. A. McCune, M. F. Kuehnel, E. Reisner, O. A. Scherman, *Chem* **2020**, *6*, 1819 – 1830; b) H. Phan, T. S. Herng, D. Wang, X. Li, W. Zeng, J. Ding, K. P. Loh, A. T. Shen Wee, J. Wu, *Chem* **2019**, *5*, 1223 – 1234; c) A. Abdurahman, T. J. H. Hele, Q. Y. Gu, J. B. Zhang, Q. M. Peng, M. Zhang, R. H. Friend, F. Li, E. W. Evans, *Nat. Mater.* **2020**, *19*, 1224—1229.

[3] T. B. Faust, D. M. D'Alessandro, *RSC Adv.* **2014**, *4*, 17498 – 17512.

[4] S. Yuan, L. Feng, K. Wang, J. Pang, M. Bosch, C. Lollar, Y. Sun, J. Qin, X. Yang, P. Zhang, Q. Wang, L. Zou, Y. Zhang, L. Zhang, Y. Fang, J. Li, H. C. Zhou, *Adv. Mater.* **2018**, *30*, 1704303.

[5] a) Z. Chen, H. Jiang, M. Li, M. O'Keeffe, M. Eddaoudi, *Chem. Rev.* **2020**, *120*, 8039 – 8065; b) F. Saraci, V. Quezada-Novoa, P. R. Donnarumma, A. J. Howarth, *Chem. Soc. Rev.* **2020**, *49*, 7949 – 7977; c) L. Zhang, S. Yuan, L. Feng, B. Guo, J.-S. Qin, B. Xu, C. Lollar, D. Sun, H.-C. Zhou, *Angew. Chem. Int. Ed.* **2018**, *57*, 5095 – 5099; *Angew. Chem.* **2018**, *130*, 5189 – 5193; d) L. Feng, Y. Wang, K. Zhang, K. Y. Wang, W. Fan, X. Wang, J. A. Powell, B. Guo, F. Dai, L. Zhang, R. Wang, D. Sun, H. C. Zhou, *Angew. Chem. Int. Ed.* **2019**, *58*, 16682 – 16690; *Angew. Chem.* **2019**, *131*, 16835 – 16843; e) Y. Wang, L. Feng, W. Fan, K. Y. Wang, X. Wang, X. Wang, K. Zhang, X. Zhang, F. Dai, D. Sun, H. C. Zhou, *J. Am. Chem. Soc.* **2019**, *141*, 6967 – 6975.

[6] D. X. Xue, A. J. Cairns, Y. Belmabkhout, L. Wojtas, Y. Liu, M. H. Alkordi, M. Eddaoudi, *J. Am. Chem. Soc.* **2013**, *135*, 7660 – 7667.

[7] a) R. Luebke, Y. Belmabkhout, L. J. Weselinski, A. J. Cairns, M. Alkordi, G. Norton, L. Wojtas, K. Adil, M. Eddaoudi, *Chem. Sci.* **2015**, *6*, 4095 – 4102; b) H. Jiang, J. Jia, A. Shkurenko, Z. Chen, K. Adil, Y. Belmabkhout, L. J. Weselinski, A. H. Assen, D. X. Xue, M. O'Keeffe, M. Eddaoudi, *J. Am. Chem. Soc.* **2018**, *140*, 8858 – 8867.

[8] a) A. H. Assen, Y. Belmabkhout, K. Adil, P. M. Bhatt, D. X. Xue, H. Jiang, M. Eddaoudi, *Angew. Chem. Int. Ed.* **2015**, *54*, 14353 – 14358; *Angew. Chem.* **2015**, *127*, 14561 – 14566; b) D. X. Xue, Y. Belmabkhout, O. Shekhah, H. Jiang, K. Adil, A. J. Cairns, M. Eddaoudi, *J. Am. Chem. Soc.* **2015**, *137*, 5034 – 5040; c) D. X. Xue, A. Cadiau, L. J. Weselinski, H. Jiang, P. M. Bhatt, A. Shkurenko, L. Wojtas, Z. Chen, Y. Belmabkhout, K. Adil, M. Eddaoudi, *Chem. Commun.* **2018**, *54*, 6404 – 6407.

[9] Y. Zhang, Y. Wang, L. Liu, N. Wei, M. L. Gao, D. Zhao, Z. B. Han, *Inorg. Chem.* **2018**, *57*, 2193 – 2198.

[10] a) J. Su, W. He, X.-M. Li, L. Sun, H.-Y. Wang, Y.-Q. Lan, M. Ding, J.-L. Zuo, *Matter* **2020**, *2*, 711 – 722; b) L. S. Xie, G. Skorupskii, M. Dinca, *Chem. Rev.* **2020**, *120*, 8536 – 8580.

[11] a) Y. Zhou, F. Yu, J. Su, M. Kurmoo, J. L. Zuo, *Angew. Chem. Int. Ed.* **2020**, *59*, 18763 – 18767; *Angew. Chem.* **2020**, *132*, 18922 – 18926; b) M. Jiang, Y. G. Weng, Z. Y. Zhou, C. Y. Ge, Q. Y. Zhu, J. Dai, *Inorg. Chem.* **2020**, *59*, 10727 – 10735.

[12] a) H. Y. Wang, J. Y. Ge, C. Hua, C. Q. Jiao, Y. Wu, C. F. Leong, D. M. D'Alessandro, T. Liu, J. L. Zuo, *Angew. Chem. Int. Ed.* **2017**, *56*, 5465 – 5470; *Angew. Chem.* **2017**, *129*, 5557 – 5562; b) J. Castells-Gil, S. Manas-Valero, I. J. Vitorica-Yrezabal, D. Ananias, J. Rocha, R. Santiago, S. T. Bromley, J. J. Baldovi, E. Coronado, M. Souto, G. Minguez Espallargas, *Chem. Eur. J.* **2019**, *25*, 12636 – 12643; c) J. Su, T. H. Hu, R. Murase, H. Y. Wang, D. M. D'Alessandro, M. Kurmoo, J. L. Zuo, *Inorg. Chem.* **2019**, *58*, 3698 – 3706.

[13] a) J. Su, S. Yuan, T. Wang, C. Lollar, J.-L. Zuo, J. Zhang, H.-C. Zhou, *Chem. Sci.* **2020**, *11*, 1918 – 1925; b) M. Souto, A. Santiago-Portillo, M. Palomino, I. J. Vitorica-Yrezabal, B. J. C. Vieira, J. C. Waerenborgh, S. Valencia, S. Navalon, F. Rey, H. Garcia, G. Minguez Espallargas, *Chem. Sci.* **2018**, *9*, 2413 – 2418.

[14] a) J. Su, S. Yuan, H. Y. Wang, L. Huang, J. Y. Ge, E. Joseph, J. Qin, T. Cagin, J. L. Zuo, H. C. Zhou, *Nat. Commun.* **2017**, *8*, 2008; b) M. Souto, J. Romero, J. Calbo, I. J. Vitorica-Yrezabal, J. L. Zafra, J. Casado, E. Orti, A. Walsh, G. Minguez Espallargas, *J. Am. Chem. Soc.* **2018**, *140*, 10562 – 10569.

[15] a) F. Pointillart, Y. L. Gal, S. Golhen, O. Cador, L. Ouahab, *Inorg. Chem.* **2009**, *48*, 4631 – 4633; b) S. S. Park, C. H. Hendon, A. J. Fielding, A. Walsh, M. O'Keeffe, M. Dinca, *J. Am. Chem. Soc.* **2017**, *139*, 3619 – 3622.

[16] a) H. Müller, S. O. Svensson, A. N. Fitch, M. Lorenzen, D. G. Xenikos, *Adv. Mater.* **1997**, *9*, 896 – 900; b) H. V. Schröder, F. Stein, J. M. Wollschlager, S. Sobottka, M. Gaedke, B. Sarkar, C. A. Schalley, *Angew. Chem. Int. Ed.* **2019**, *58*, 3496 – 3500; *Angew. Chem.* **2019**, *131*, 3534 – 3538; c) F. Pointillart, B. Le Guennic, S. Golhen, O. Cador, L. Ouahab, *Chem. Commun.* **2013**, *49*, 11632 – 11634.

[17] a) B. Li, Y. M. Zhao, A. Kirchon, J. D. Pang, X. Y. Yang, G. L. Zhuang, H. C. Zhou, *J. Am. Chem. Soc.* **2019**, *141*, 6822 – 6826; b) L. Yang, X. He, M. Dinca, *J. Am. Chem. Soc.* **2019**, *141*, 10475 – 10480; c) S. V. Potts, L. J. Barbour, D. A. Haynes, J. M. Rawson, G. O. Lloyd, *J. Am. Chem. Soc.* **2011**, *133*, 12948 – 12951; d) K. A. Collins, R. J. Saballos, M. S. Fataftah, D. Puggioni, J. M. Rondinelli, D. E. Freedman, *Chem. Sci.* **2020**, *11*, 5922 – 5928; e) D. Maspoch, D. Ruiz-Molina, K. Wurst, N. Domingo, M. Cavallini, F. Biscarini, J. Tejada, C. Rovira, J. Veciana, *Nat. Mater.* **2003**, *2*, 190 – 195.

[18] a) T. C. Narayan, T. Miyakai, S. Seki, M. Dinca, *J. Am. Chem. Soc.* **2012**, *134*, 12932 – 12935; b) L. S. Xie, E. V. Alexandrov, G. Skorupskii, D. M. Proserpio, M. Dinca, *Chem. Sci.* **2019**, *10*, 8558 – 8565; c) A. Cadiau, L. S. Xie, N. Kolobov, A. Shkurenko, M. Qureshi, M. R. Tchalala, S. S. Park, A. Bavykina, M. Eddaoudi, M. Dincă, C. H. Hendon, J. Gascon, *Chem. Mater.* **2020**, *32*, 97 – 104.

[19] A. L. Spek, *Acta Crystallogr. Sect. C* **2015**, *71*, 9 – 18.

[20] D. Choudhury, B. Das, D. D. Sarma, C. N. R. Rao, *Chem. Phys. Lett.* **2010**, *497*, 66 – 69.

[21] a) C. Hua, P. W. Doheny, B. Ding, B. Chan, M. Yu, C. J. Kepert, D. M. D'Alessandro, *J. Am. Chem. Soc.* **2018**, *140*, 6622 – 6630; b) G. Chen, J. Sun, Q. Peng, Q. Sun, G. Wang, Y. Cai, X. Gu, Z. Shuai, B. Z. Tang, *Adv. Mater.* **2020**, *32*, 1908537.

[22] a) B. L. Huang, Z. Ni, A. Millward, A. J. H. McGaughey, C. Uher, M. Kaviany, O. Yaghi, *Int. J. Heat Mass Transfer* **2007**, *50*, 405 – 411; b) L. Sun, B. Liao, D. Sheberla, D. Kraemer, J. Zhou, E. A. Stach, D. Zakharov, V. Stavila, A. A. Talin, Y. Ge, M. D. Allendorf, G. Chen, F. Léonard, M. Dincă, *Joule* **2017**, *1*, 168 – 177.

[23] a) J. Espín, L. Garzón-Tovar, A. Carné-Sánchez, I. Imaz, D. Maspoch, *ACS Appl. Mater. Interfaces* **2018**, *10*, 9555 – 9562; b) Q. Ma, P. Yin, M. Zhao, Z. Luo, Y. Huang, Q. He, Y. Yu, Z. Liu, Z. Hu, B. Chen, H. Zhang, *Adv. Mater.* **2019**, *31*, 1808249.

Manuscript received: October 16, 2020
Revised manuscript received: November 24, 2020
Accepted manuscript online: November 25, 2020
Version of record online: January 4, 2021

